7. S.-J. Lin and V. Cizewski Culotta, *ibid*., p. 3748.
8. S.-J. Lin, R. A. Pufahl, A. Dancis, T. V. O'Halloran, V. Cizewski Culotta, *J. Biol. Chem.* **272**, 9214 (1997).
9. L. W. J. Klomp *et al*., *ibid*., p. 9221.
10. C. Vulpe *et al*., *Nature Genet.* **3**, 7 (1993).
11. P. C. Bull *et al*., *ibid.* **5**, 327 (1993); R. E. Tanzi *et al*., *ibid*., p. 344.
12. S. Lutsenko and J. H. Kaplan, *Biochemistry* **34**, 15607 (1995).
13. M. J. Petris *et al*., *EMBO J.* **15**, 6084 (1996).
14. P. C. Bull and D. W. Cox, *Trends Genet.* **10**, 246 (1994); P.-O. Eriksson and L. Sahlman, *J. Biomol. NMR* **3**, 613 (1993); J. L. Hobman and N. L. Brown, in *Metal Ions in Biological Systems*, A. Sigel and H. Sigel, Eds. (Dekker, New York, 1997), vol. 34, pp. 527–568.
15. *ATX1* was cloned into pET11d (Novagen) and expressed in *E. coli* strain BL21(DE3) after induction with IPTG. The protein was isolated by a freeze-thaw extraction and purified to homogeneity by DEAE-Sephacel batch treatment and subsequent chromatography on CM Sepharose FF (Pharmacia). Approximately 6 to 10 mg of pure protein was obtained per liter of bacterial culture. Protein concentration was determined from absorbance at 280 nm (with an extinction coefficient of 4400 M^{-1} cm^{-1}, calculated on the basis of total amino acid composition) or by Bradford assay [M. Bradford *Anal. Biochem.* **72**, 248 (1976)] with immunoglobulin G as a standard. Electrospray mass spectrometry (ES-MS) of apo-Atx1 revealed a single peak of 8088.1 daltons, which corresponds to full-length Atx1 lacking its NH_2-terminal methionine; in addition, ES-MS of Hg-Atx1 yielded one peak at 8287.6 daltons. Gel filtration on an HPLC QC-PAK TSK 200GL (TosoHaas) column yielded molecular sizes of 10,200, 9840, and 9960 daltons for apo-, Hg(II)-, and Cu(I)-Atx1, respectively.
16. Cu(I)-Atx1 was typically prepared by incubation of apoprotein with a Cu(II) salt in the presence of a thiol reductant. All manipulations were performed in an inert atmosphere at 4°C. $CuSO_4$ (2.5 equivalents) was added, with stirring, to a solution of apo-Atx1 and DTT (20-fold molar excess relative to protein) in 50 mM tris (pH 8.0, adjusted with solid MES to avoid Cl^-). Excess metal was removed by ultrafiltration and the protein was exchanged into a solution containing 20 mM MES (pH 6.0) and 20% (v/v) glycerol. The final protein concentration was 7.84 mM with a Cu/protein ratio of 0.75 ± 0.02. Solutions (>2 mM) of the Cu(I)-protein can be handled in air at 4°C for 30 min or stored long term (>4 months) at −70°C with no observable formation of Cu(II).
17. XAS data were obtained at Stanford Synchrotron Radiation Laboratory (SSRL) beam line VII-3 as fluorescence excitation spectra with a Ge solid-state detector array. Samples (150 μl) were maintained at 10 K throughout measurements. Data reduction and analysis were performed according to standard procedures [P. J. Riggs-Gelasco, R. Mei, C. F. Yocum, J. E. Penner-Hahn, *J. Am. Chem. Soc.* **118**, 2387 (1996)]. Data were fitted with amplitude and phase functions calculated with FEFF 6.01 [J. J. Rehr *et al*., *ibid.* **113**, 5135 (1991)], calibrated by fitting model compounds of known structure.
18. L.-S. Kau *et al*., *ibid.* **109**, 6433 (1987).
19. D. R. Winge *et al*., *J. Bioinorg. Chem.* **2**, 2 (1997).
20. E. I. Solomon *et al*., *Chem. Rev.* **96**, 2563 (1996).
21. H. H. Thorp, *Inorg. Chem.* **31**, 1585 (1992).
22. I. J. Pickering *et al*., *J. Am. Chem. Soc.* **115**, 9498 (1993).
23. D. Coucouvanis *et al*., *Inorg. Chem.* **19**, 2993 (1980).
24. S. A. Koch *et al*., *ibid.* **23**, 122 (1984).
25. ^{199}Hg-Atx1 was prepared by the addition of ^{199}Hg(II) to apo-Atx1 in 20 mM MES (pH 6.0). DTT was removed from apo-Atx1 by ultrafiltration before the addition of mercury. ^{199}Hg(II) (1.2 equivalents) was added to apo-Atx1 on ice with stirring. Free metal was removed with several successive washes with buffer by ultrafiltration followed by exchange into D_2O buffer. The final protein concentration was 2.40 mM with a ^{199}Hg/protein ratio of 0.83 ± 0.05 in a solution containing 25 mM sodium phosphate (pH* 6.6), 50 mM NaCl, and 98% D_2O. A similar protocol was used to prepare the EXAFS sample except that Cl^- was not present in any of the buffers. The final protein concentration was 3.36 mM with a Hg/protein ratio of 0.75 ± 0.06 in 20 mM MES (pH 6.0).
26. J. G. Wright *et al*., *Prog. Inorg. Chem.* **38**, 323 (1990).
27. L. M. Utschig *et al*., *Science* **268**, 380 (1995).
28. L. M. Utschig *et al*., *Inorg. Chem.* **36**, 2926 (1997).
29. The $^1H\{^{199}Hg\}$ HMQC spectra of ^{199}Hg-Atx1 were obtained on a Bruker 600-MHz spectrometer (14.09 T, 107.4 MHz for ^{199}Hg) equipped with a 5-mm tunable probe. The pulse sequence and optimal delays for Met, Cys, and His ligands have been described (*27*). Spectral widths of 7246 Hz for ^{1}H (*F2*) and 32,221 Hz for ^{199}Hg (*F1*) were used. A total of 64 t_1 blocks was accumulated, with 1024 transients collected in *F2* per block. The ^{1}H 90° pulse was 8.0 μs and the $^{199}Hg(90°)^{-1}$ value was 20.4 μs, as calibrated with $Hg(CH_3)_2$. Safety note: The latter compound is permeable to latex gloves and is exceedingly toxic. Discussion of alternative compounds can be found at www.chem.nwu.edu/~ohallo/HgNMRStandards
30. G. R. Dieckmann *et al*., *J. Am. Chem. Soc.* **119**, 6195 (1997).
31. J. R. R. Frausto da Silva and R. J. P. Williams, in *The Biological Chemistry of the Elements* (Clarendon, Oxford, 1991), pp. 396–397.
32. B. V. Cheesman, A. P. Arnold, D. L. Rabenstein, *J. Am. Chem. Soc.* **110**, 6359 (1988).
33. The two-hybrid analysis [L. Guarente, *Proc. Natl. Acad. Sci. U.S.A.* **90**, 1639 (1993)] was performed with the MATCHMAKER System (Clontech). Nucleotides +1 to +222 of *ATX1* were amplified by PCR and inserted at the Bam HI and Pst I sites of the pGBT9 plasmid encoding the DNA-binding domain of Gal4, to yield pPS002. For preparation of vector pPS001, *CCC2* nucleotides (nt) +1 to +745 were amplified and inserted at the Eco RI and Sal I sites of pGAD424 encoding the Gal4 activation domain. The remaining three Ccc2-Gal4 fusion constructs were obtained by amplifying the corresponding *CCC2* sequences and inserting them into the Bam HI and Pst I sites of pGAD424. Plasmid pCF12 contains *CCC2* nt +1163 to +1582, pCF34 contains nt +1731 to +2711, and pCF56 contains nt +2831 to +3294. Yeast strain SFY526 was cotransformed with the vectors based on pGBT9 and pGAD424, and grown in 5 ml of synthetic dextrose (SD) medium to an optical density at 600 nm of 4.0. Cells were harvested, washed in water, and resuspended in 1 ml of 50 mM sodium phosphate buffer (pH 7.0) containing 10 mM KCl, 1 mM $MgSO_4$, and 40 mM β-mercaptoethanol. They were lysed by homogenization with glass beads after adding 45 μl of 0.1% SDS. The resulting extract (800 μl) was mixed with 200 μl of *o*-nitrophenyl-β-D-galactopyranoside (4 mg/ml) and incubated at 30°C overnight. After centrifugation, β-Gal activity was measured in the supernatant at 420 nm. In some instances, cells were grown in the presence of the Cu chelator BCS (3 mM). Results are representative of two to four independent samples with ranges of ≤15%. β-Gal activity units for the p53/SV40 positive controls (and vectors) were 9.75 (0.21) in the absence of BCS and 9.95 (0.27) in the presence of BCS.
34. R. P. Hausinger *et al*., Eds., *Mechanisms of Metallocenter Assembly* (VCH, New York, 1996).
35. R. A. Steele and S. J. Opella, *Biochemistry* **36**, 6885 (1997).
36. J. Gitschier and W. Fairbrother, personal communication.
37. V. Cizweski Culotta *et al*., *J. Biol. Chem.* **272**, 23469 (1997).

38. Supported by NIH: GM-54111 (T.V.O.), GM-38047 (J.E.P.-H.), GM-50016 (V.C.C.), Biophysics Training Grant T32GM08382 (C.P.S.), Training Grant ES 07141 (P.J.S.), and F32 DK-09305 (R.A.P.). SSRL is funded by the Department of Energy (Office of Basic Energy Sciences and Office of Health and Environmental Research) and by the NIH Biomedical Research Technology Program. The Northwestern University 600-MHz NMR Facility is funded by the W. M. Keck Foundation, NSF, NIH, and the R. H. Lurie Cancer Center. We thank R. Scott for the $Cu(SC_6H_5)_3^{2-}$ XANES data, D. Huffman for $[Cu(II)(imidazole)_4](NO_3)_2$, and A. Duncan for the color illustration.

19 May 1997; accepted 4 September 1997

Measurement of the Force-Velocity Relation for Growing Microtubules

Marileen Dogterom* and Bernard Yurke

Forces generated by protein polymerization are important for various forms of cellular motility. Assembling microtubules, for instance, are believed to exert pushing forces on chromosomes during mitosis. The force that a single microtubule can generate was measured by attaching microtubules to a substrate at one end and causing them to push against a microfabricated rigid barrier at the other end. The subsequent buckling of the microtubules was analyzed to determine both the force on each microtubule end and the growth velocity. The growth velocity decreased from 1.2 micrometers per minute at zero force to 0.2 micrometer per minute at forces of 3 to 4 piconewtons. The force-velocity relation fits well to a decaying exponential, in agreement with theoretical models, but the rate of decay is faster than predicted.

It has long been speculated that the assembly and disassembly of cytoskeletal filaments, such as microtubules (MTs) and actin, can generate forces that are important for various forms of cellular motility. Examples include the motions of chromosomes during mitosis that depend on both the assembly and disassembly of MTs (*1, 2*), actin-dependent motility such as cell crawling and the propulsion of *Listeria* through a host cell (*3*), and possibly the MT-dependent transport of intracellular membranes (*4*). To understand the role of force production by protein polymerization in vivo, it is important to determine the maximum forces that can be generated and the effect of an opposing force on the assembly dynamics of

Bell Laboratories, Lucent Technologies, 600 Mountain Avenue, Murray Hill, NJ 07974, USA.

*To whom correspondence should be addressed. Present address: F.O.M. Institute AMOLF, Kruislaan 407, 1098 SJ Amsterdam, Netherlands.

a protein polymer. In the case of MTs, there is clear experimental evidence that both their assembly (*4–6*) and disassembly (*7*) can generate force, but limited quantitative data are available on the actual magnitude of these forces. In this respect, the study of force production by the assembly of cytoskeletal filaments, or by protein aggregation in general, clearly lags behind the study of force production by motor proteins, for which a number of quantitative in vitro assays have been developed (*8*).

We created an experimental system in which growing MTs were made to push against an immobile barrier, and analyzed the subsequent buckling of the MTs to study the forces that were produced; the force calibration was provided by a measurement of the flexural rigidity of the MTs (*9*). We etched arrays of long channels (30 μm wide, 1 μm deep) in glass cover slips (*10*); the walls of these channels were used as barriers. Using materials with different etch rates, we produced walls with an "overhang" that prevented the MTs from sliding upward along the wall (Fig. 1, A and B). Short stabilized MT seeds, labeled with biotin, were attached to the bottom of the streptavidin-coated channels, and MTs were allowed to grow from these seeds (Fig. 1A) (*11*). Because the seeds were randomly positioned in the channels, the MTs approached the walls from different angles and distances. We scanned our samples for MTs that were growing roughly perpendicular to the walls and observed them as their growing ends approached the walls (Fig. 1, C and D) (*12*).

In many cases, the MT end was caught underneath the overhang on the wall, forcing the MT to encounter the wall. After encountering the wall, most MTs continued to increase in length, indicating a continuing addition of tubulin dimers at the growing MT ends. The virtually incompressible (*9*) MTs were observed to bend in two different ways to accommodate this continuing increase in length. In some cases, the MT end moved along the side of the wall while the MT bent roughly perpendicular to its original direction [these MTs were not followed any further (*13*)]. In other cases, the MT end, probably hindered by small irregularities in the shape of the wall, did not move along the side of the wall; this caused the MT to buckle with its end pivoting around a fixed contact point with the wall (Fig. 1, C and D). The force exerted by these MTs on the wall was large enough to overcome the critical buckling force (*14*).

After the initiation of buckling, both the magnitude and the direction of the force f exerted by each MT on the wall (and therefore by the wall on the MT) were solely determined by the elastic restoring force of the buckled MT [initially this force should be roughly equal to the critical buckling force (*14*)]. A considerable component f_p of this force was directed parallel to the direction of elongation of the MT, thereby opposing its growth (Fig. 2). Assuming that a MT behaves as a homogeneous elastic rod, the magnitude of the critical buckling force f_c normalized by the flexural rigidity κ of the MT is given by $f_c/\kappa = A/L^2$, where L is the length of the MT. The prefactor A depends on the quality of the clamp provided by the seed: $A \approx 20.19$ (the maximum value) for a perfect clamp that fixes the initial direction of the MT exactly in the direction of the contact point with the wall, $A = \pi^2$ (the minimum value) for a seed that acts as a hinge around which the MT is completely free to pivot. Because there was no reason to assume that either of these conditions would be perfectly met, we expected buckling forces somewhere between these minimum and maximum values.

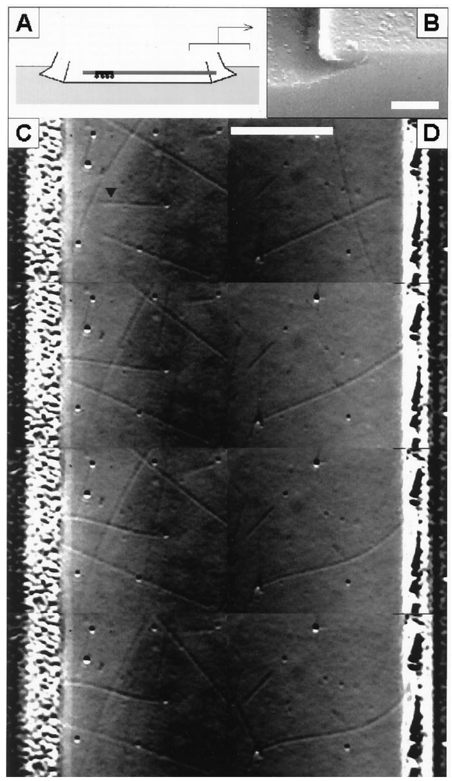

Fig. 1. In vitro assay to study the force exerted by a single growing MT. (**A**) Schematic representation of the experiment (shown in perspective from a side view; not to scale). A biotinylated MT seed (black), attached to the streptavidin-coated bottom of a channel (indicated by black dots), templates the growth of a freely suspended MT (gray). An overhang was created on the walls of the channel to prevent the MT ends from sliding upward after encountering the wall. (**B**) Electron microscopy image showing a wall with overhang (scale bar, 1 μm). (**C** and **D**) DIC images of two buckling MTs (top view) (*12*). The upper panels each show a MT [arrowhead in top left of (C)] growing from a randomly positioned seed. The lower panels are snapshots (separated by 1 min) of each MT after the growing end has encountered the wall. Because of the contrast produced by the overhang on the walls (which vary in size between samples), the last few micrometers of the MTs cannot be seen. The sharp changes in contrast indicate the actual locations of the walls. Scale bar, 10 μm.

To determine the actual force acting on each buckling MT, we obtained a sequence of fits to the shape of an elastic rod from video frames spaced 2 s apart (Fig. 2) (*15*). When no assumptions were made about the quality of the clamp or the magnitude of f_c, these fits produced values for f/κ, f_p/κ, and L as a function of time. Fig. 3A shows the parallel component of the normalized force and the MT length as a function of time for five different examples, both before and after reaching the wall. The MT length before reaching the wall was determined by tracking the end of the growing MT (*15*)

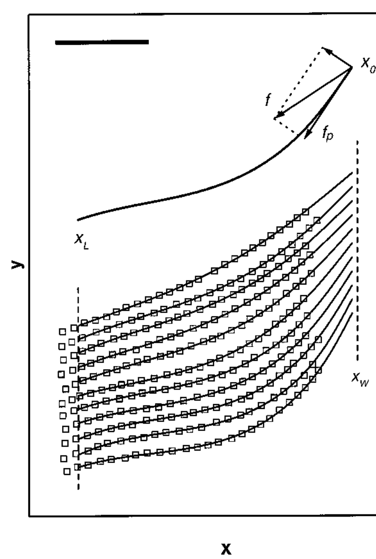

Fig. 2. Analysis of MT buckling shapes (*15*). Open squares show the hand-recorded shapes of the MT shown in Fig. 1D at 12-s intervals (shapes were analyzed at 2-s intervals). The dashed line on the left indicates the position of the seed (x_L). The dashed line on the right indicates the position of the wall (x_W) as judged by eye from the images (Fig. 1D). The solid lines show fits to the shape of an elastic rod. One (at the top) is shown as an example. We assumed that the MT was held at its seed and that a force f was applied at the contact point of the MT with the wall (x_0, y_0). This contact point remained fixed in time and was chosen to produce the best combined fit over the entire time sequence (this produces a value of x_0 very close to x_W). We further assumed that the MT was free to pivot around the contact point, but we made no assumptions about the quality of the clamp provided by the seed. The fits produced the magnitude and the direction of the force f (normalized by the flexural rigidity κ of the MT) at each time point, as well as the length of the MT given by the arc length between x_0 and x_L. MT growth is opposed by f_p, the component of the force that is directed parallel to the axis of the MT. Scale bar, 5 μm.

(in each case a segment in the time sequence is missing, during which the end of the MT was obscured by the presence of the overhang on the wall). The growth velocity varied considerably even at zero force, as reported previously (*16, 17*). However, all MTs clearly slowed as soon as a force was applied. These curves also show that the forces on short buckling MTs tend to be greater than the forces on long buckling MTs. The total normalized force (not just the parallel component) as a function of MT length is shown in Fig. 3B for all MT shapes analyzed. For each MT length, the forces vary over a certain range because of variability in the quality of the clamp provided by the seed. The two dotted lines indicate the theoretical limits for f_c (discussed above); as expected, we found that the restoring forces were between these limits, which validated our assumption that MTs behave as homogeneous elastic rods.

In Fig. 4 the average growth velocity $\langle v \rangle$ is plotted as a function of force (the force-velocity curve) for all data combined (*18*). This plot shows that the growth velocity approaches the velocity of a freely growing MT (~1.2 μm min^{-1}) at low force, and decreases to ~0.2 μm min^{-1} as more and more force is applied. This implies that the reduction in growth velocity is controlled by the applied force and is not simply caused by the proximity of the end of the MT to the glass barrier. The lower *x* axis in Fig. 4 is labeled with values for the normalized force because this is the parameter obtained from our fits. An independent measure of κ is needed to obtain values for the absolute force. The flexural rigidity of pure MTs has been measured using various methods; the values reported range over an order of magnitude, 4 to 40 pN·μm^2 (*6, 19, 20*). We used an analysis of the thermal fluctuations to measure the rigidity of our MTs (*21*) and found values at the upper end of this range: 34 ± 7 pN·μm^2. This means that the largest forces in Fig. 4 are on the order of 4 pN (the upper *x* axis is labeled with absolute values of force derived from our measurement of the flexural rigidity).

The force-velocity relation in Fig. 4 can be compared with theoretical predictions. In the absence of force, the growth velocity is given by the difference in the rate of addition and removal of subunits, $v = \delta(\alpha c - \beta)$, where δ is the added MT length per dimer (δ = δ/13 nm for an MT with 13 protofilaments), α*c* is the rate of subunit addition (the on-rate), *c* is the tubulin concentration, and β is the rate of subunit removal (the off-rate). In principle, both α and β may be affected by a force that opposes elongation of the MT (f_p in our case). Thermodynamic arguments (*22*) show that their ratio (which gives the critical tubulin concentration c_{cr}) must increase with force according to

$$c_{cr}(f_p) = \frac{\beta(f_p)}{\alpha(f_p)} = \frac{\beta(0)}{\alpha(0)} \exp(f_p\delta/k_BT) \qquad (1)$$

where k_B is the Boltzmann constant and T is temperature. This leads to

$$v(f_p) = \delta\{\alpha \exp(-qf_p\delta/k_BT)c - \beta \exp[(1-q)f_p\delta/k_BT]\} \qquad (2)$$

where *q* may take any value between 0 and 1 (possibly in a force-dependent way). The stall force f_s (the force at which the velocity becomes equal to zero) is independent of *q* and is given by

$$f_s = \frac{k_BT}{\delta} \ln \frac{\alpha c}{\beta} \qquad (3)$$

A similar result is obtained if the growth process is pictured as a "Brownian ratchet" (*23*). In this more mechanistic view, the on-rate depends on the force-dependent probability that thermal fluctuations (in the position of the MT end in this case) allow for a gap between the MT end and the barrier that is large enough for a dimer to attach to the growing MT end (under optimal conditions, the size of this gap along the direction of MT growth is equal to δ, the added length per dimer). If the force is independent of the size of the gap and the time required to add a dimer is long relative to the time required for the MT end to diffuse over a distance δ, then

$$v(f_p) = \delta[\alpha \exp(-f_p\delta/k_BT)c - \beta] \qquad (4)$$

(*23, 24*). This relation assumes that the effect of force on the off-rate can be neglected. We performed a weighted least-squares fit of the data in Fig. 4 to both the function $v(f_p) = A - B\exp(Cf_p/\kappa)$ (assuming that only the off-rate is affected or $q = 0$) and the function $v(f_p) = A\exp(-Cf_p/\kappa) - B$ (assuming that only the on-rate is affected or $q = 1$), where *A*, *B*, and *C* are fitting parameters. In the first case, the best fit ($\chi^2 = 1.5$)

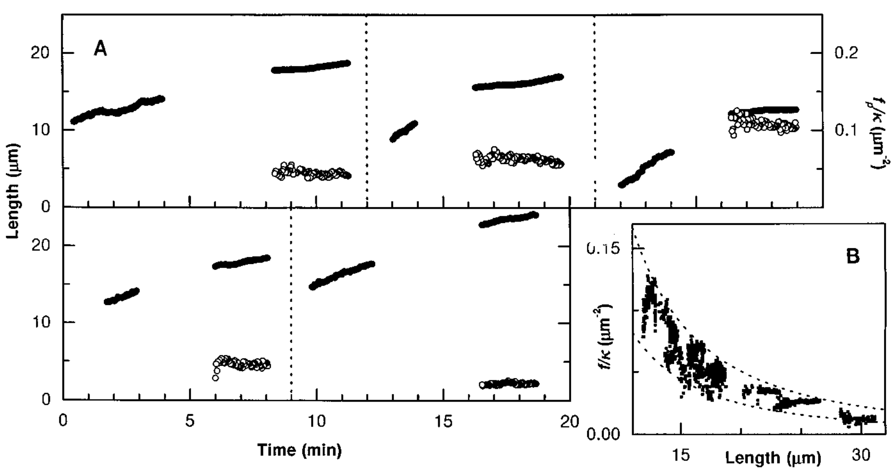

Fig. 3. MT length and applied force obtained from the analysis of MT buckling shapes such as shown in Fig. 2. (**A**) For five different MTs, the length *L* as a function of time (at 2-s intervals) is shown both before and after contact with the wall (solid symbols). A segment of time is missing in each case, during which the end of the growing MT was obscured by the presence of the overhang on the wall. Open symbols show the parallel component of the normalized force, f_p/κ. The lower left curve corresponds to the MT shown in Figs. 1D and 2. The upper right curve corresponds to the MT shown in Fig. 1C. (**B**) Total normalized force, f/κ, as a function of MT length for all MT shapes analyzed (n = 1316). Each point corresponds to one MT shape. The dashed lines indicate the theoretical length dependence of f_c in two limiting cases: $f_c/\kappa = 20.19/L^2$ for a MT with a seed that acts as a perfect clamp (upper curve) and $f_c/\kappa = \pi^2/L^2$ for a MT with a seed that acts as a perfect hinge (lower curve). In the experiments, the seeds behaved in an intermediate way and, as expected, the forces obtained from the fits fall between these two limiting curves.

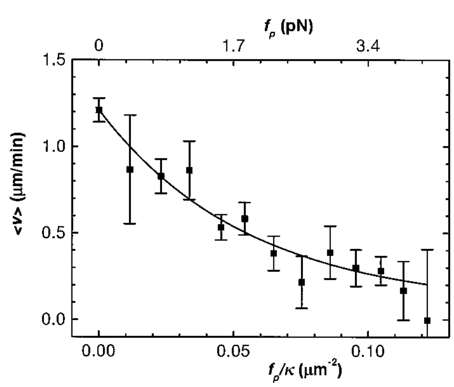

Fig. 4. Average MT growth velocity as a function of force. Velocity and force were obtained from combining data such as shown in Fig. 3A (*18*). The lower *x* axis gives the value of the normalized force, f_p/κ. The upper *x* axis gives the absolute value of the force, based on our measurement of the flexural rigidity. The solid line gives the best fit of the data to an exponential decay.

produced extremely large values for the parameters A and B, and a value for C nearly equal to zero (corresponding to almost a straight line). Experimental results show, however, that B is very small in the absence of force (*25*). Fixing the maximum value of B at 0.5 μm min^{-1} produced a fit that was much worse ($\chi^2 = 2.5$), and smaller values of B produced fits that were even worse. Consequently, it is unlikely that the only effect of force is an increase in the off-rate. In the second case, a more reasonable result (indicated by the solid line in Fig. 4) was obtained: $\chi^2 = 0.43$ with $A = 1.13 \pm 0.11$ μm min^{-1}, $B = -0.08 \pm 0.12$ μm min^{-1}, and $C = 18 \pm 4$ μm^2. This indicates the possibility that the only effect of force is a decrease in the on-rate (*26*). Although B is expected to be small, its true value should be greater than zero. Because of the uncertainty in B, it is impossible to extract a good estimate of f_s from this fit.

The value predicted for the parameter C is equal to $\kappa\delta / k_B T$, which, given our measured value for κ, corresponds to 5 ± 1 μm^2. This is smaller than the value obtained from the fit for $q = 1$, 18 ± 4 μm^2, which implies that the growth velocity decreases faster with force than would be expected from theoretical arguments [this discrepancy becomes even larger if we assume a smaller value for q (*26*)]. The theoretical rate corresponds to an optimum situation in which the free energy available from the assembly of all 13 protofilaments is converted into mechanical work. Despite the relatively large experimental error bars, our data indicate that this is not the case under our conditions. It may be that, if the end of a growing MT is not blunt but pointed, only a few protofilaments are supporting the load. If this is pictured as a ratchet, gaps closer to the size of a full dimer may be required to squeeze in the next subunit, which would increase the predicted value for C. Also, growth may occur through the closure of a sheet of protofilaments (*17*), which could make the gap size needed for this process even larger than the size of a dimer.

We have presented a quantitative method for studying the force that can be produced by a single growing MT in interaction with a nonspecific glass barrier. Considering that under these conditions less force is produced than is theoretically possible, a logical next step would be to study whether the interaction of the growing MT end with a specific attachment site modifies this result. In principle it should be possible to coat the walls [or simply a pattern of lines (*27*)] with isolated chromosomes (*7*) or kinetochore constructs (*28*) and repeat the same experiment. This system can also be used to study the effect of force on the catastrophe frequency of MTs (the probability of switching from the growing to the shrinking state). In our experiments, growth often persisted after the initiation of buckling, which implies that an opposing force does not markedly increase the catastrophe frequency. Quantitatively verifying this possibility would require the observation of many catastrophe events both before and during the application of force.

REFERENCES AND NOTES

1. S. Inoué and H. Sato, *J. Gen. Physiol.* **50**, 529 (1967).
2. S. Inoué and E. D. Salmon, *Mol. Biol. Cell* **6**, 1619 (1995).
3. L. Cramer, T. Mitchison, J. Theriot, *Curr. Opin. Cell Biol.* **6**, 82 (1994).
4. C. M. Waterman-Storer, J. Gregory, S. F. Parsons, E. D. Salmon, *J. Cell Biol.* **130**, 1161 (1995).
5. H. Hotani and H. Miyamoto, *Adv. Biophys.* **26**, 135 (1990).
6. M. Elbaum, D. Kuchnir Fygenson, A. Libchaber, *Phys. Rev. Lett.* **76**, 4078 (1996); D. Kuchnir Fygenson, M. Elbaum, B. Shraiman, A. Libchaber, *Phys. Rev. E* **55**, 850 (1997).
7. D. E. Koshland, T. J. Mitchison, M. W. Kirschner, *Nature* **331**, 499 (1988); M. Coue, V. A. Lombillo, J. R. McIntosh, *J. Cell Biol.* **112**, 1165 (1991); V. A. Lombillo, R. J. Stewart, J. R. McIntosh, *Nature* **373**, 161 (1995).
8. K. Svoboda and S. M. Block, *Cell* **77**, 733 (1994); A. J. Hunt, F. Gittes, J. Howard, *Biophys. J.* **67**, 766 (1994); J. T. Finer, R. M. Simmons, J. A. Spudich, *Nature* **368**, 113 (1994); A. Ishijima *et al.*, *Biophys. J.* **70**, 383 (1996).
9. F. Gittes, E. Meyhofer, S. Baek, J. Howard, *Biophys. J.* **70**, 418 (1996).
10. Clean cover slips were coated with photoresist. Then, a pattern of 25-μm-wide lines, separated by 30 μm, was made using standard photolithography techniques (*29*). A 0.3-μm layer of SiO was vapor-deposited under vacuum (5×10^{-6} torr), followed by a 20-nm layer of chromium. The remaining photoresist was stripped in acetone and the samples were immersed in buffered hydrofluoric acid for 7 min. This produced channels 1 μm deep and 30 μm wide, with "overhangs" on the walls resulting from the slow etching of SiO as compared with glass (see Fig. 1B). The remaining chromium was stripped and the samples were cleaned and stored in ethanol.
11. Tubulin was purified from bovine brain by two cycles of polymerization-depolymerization followed by phosphocellulose chromatography [T. Mitchison and M. Kirschner, *Nature* **312**, 237 (1984)]. Stable seeds were prepared (*29*) from 88% unlabeled, 7% rhodamine-labeled, and 5% biotin-labeled tubulin [A. Hyman *et al.*, *Methods Enzymol.* **196**, 478 (1991)]. Cover slips with etched channels were incubated for 5 min on a drop of streptavidin (0.2 mg/ml in BRB80, a buffer derived from Brinkley reassembly buffer containing 80 mM K-Pipes, 1 mM EGTA, and 1 mM $MgCl_2$), rinsed with distilled water, and left to air-dry. Slides were coated in the same way with α-casein (5 mg/ml in BRB80) to minimize sticking. A solution containing unlabeled tubulin (25 μM in BRB80) supplemented with 1 mM guanosine triphosphate, 2 mM $MgCl_2$, MT seeds, and an oxygen scavenging system [4 mM dithiothreitol, catalase (0.2 mg/ml), glucose oxidase (0.4 mg/ml), and 50 mM glucose] was squashed firmly between slide and cover slip. The sample was sealed with paraffin and held at a constant temperature of 22°C on the microscope stage (*12*). Catastrophes were often observed under these conditions, and growth from the minus-end of the seeds was rare.
12. Samples were viewed by video-enhanced differential interference contrast (DIC) microscopy (Nikon Diaphot with Paultek charge-coupled device camera). The oil immersion objective (60×) was held at constant temperature (22°C) and the condenser was used without oil to keep the sample temperature coupled to that of the objective. Background subtraction, two-frame averaging, and contrast enhancement were performed online (Omnex, Imagen) and images were recorded on videotape. For MT tracking and shape analysis, frames were digitized (Perceptics Pixelbuffer) and stored on a Macintosh computer.
13. M. Dogterom and B. Yurke, data not shown.
14. L. D. Landau and E. M. Lifschitz, *Theory of Elasticity* (Pergamon, New York, 1986).
15. MT shapes were analyzed from the first moment a MT was clearly buckled until it either experienced a catastrophe or the MT end started moving along the side of the wall. MTs whose ends started moving within 10 s were not analyzed. With a computer mouse, 20 to 30 points defining the shape of each MT were recorded by hand (Fig. 2). These shapes were superimposed to find the position of the seed, x_L. Between x_L and the wall, the shape of each MT was fitted (*9*) to the shape of a homogeneous elastic rod described by (*9, 14*):

$$\ell \sqrt{f/\kappa} = \int_{\varphi(0)}^{\varphi(\ell)} \frac{d\varphi}{\sqrt{1 - k^2 \sin^2 \varphi}} = F[\varphi(\ell),k] - F[\varphi(0),k] \tag{5}$$

with

$$k \sin \varphi(\ell) = \sin \frac{1}{2} [\theta(\ell) - \phi_f] \tag{6}$$

where ℓ is the arc length of the MT ($\ell = 0$ at the wall), $\theta(\ell)$ is the tangent angle along the MT, f is the magnitude of the force, ϕ_f is its direction, and κ is the flexural rigidity of the MT. $F(\varphi,k)$ is the incomplete elliptic integral of the first kind with modulus k. We assumed that the MT is free to pivot around the fixed contact point (x_0,y_0) with the wall [$\theta'(0) = 0$]. An initial guess was made for the contact point and adjusted to find the best combined fit for 10 to 12 MT shapes in the sequence (equally spaced in time). The distance between the final x_0 and x_W, the position of the wall judged from the contrast in the image, was determined to be not more than 0.5 μm. For each MT shape the fit produced values for k, ϕ_f, and f/κ. The component of the force parallel to the axis of the MT is given by $f_p = f \cos[\theta(0) - \phi_f]$. The arc length between x_0 and x_L was taken as the length L of the MT. The results for four MTs were rejected, two because of a bad fit and two because they were curved before encountering the wall and appeared to grow twice as fast after encountering the wall. Before contact with the wall, the ends of freely growing MTs were tracked by eye with a computer mouse, and the MT length was determined as the distance between the MT end and the position of the seed. Not all MT ends that approached the wall were caught underneath the overhang on the wall; some of the MTs that were caught stopped growing because they were too short to buckle under their polymerization force (none of these MTs were followed any further).
16. R. F. Gildersleeve, A. R. Cross, K. E. Cullen, A. P. Fagen, R. C. Williams, *J. Biol. Chem.* **267**, 7995 (1992).
17. D. Chrétien, S. D. Fuller, E. Karsenti, *J. Cell Biol.* **129**, 1311 (1995).
18. The changes in MT length and the applied forces were extracted for each 2-s time interval from data such as shown in Fig. 3A (total of 24 MTs, 1292 intervals). The results were binned according to force, and within each force interval the corresponding MT length changes were averaged to give the average growth velocity and its standard error. The uncertainty in the estimate of the average growth velocity is attributable to measurement errors and to variability in the growth velocity [F. Verde, M. Dogterom, E. Stelzer, E. Karsenti, S. Leibler, *J. Cell Biol.* **118**, 1097 (1992)]. The velocity at zero force was calculated from data taken before contact with the wall (total of 23 MTs, 2309 intervals). To address the concern that we might be overestimating the velocity at high force (because MTs that stall do not buckle and cannot be analyzed), we checked our video recordings for stalling MTs. We found only one that was within the length range (and therefore the force range) of the other MTs we analyzed, so we assume that we are not

seriously overestimating the velocities.
19. F. Gittes, B. Mickey, J. Nettleton, J. Howard, *J. Cell Biol.* **120**, 923 (1993); P. Venier, A. C. Maggs, M.-F. Carlier, D. Pantaloni, *J. Biol. Chem.* **269**, 13353 (1994); *ibid.* **270**, 17056 (1995); J. C. Kurz and R. C. Williams Jr., *Biochemistry* **34**, 13374 (1995); H. Felgner, R. Frank, M. Schliwa, *J. Cell Sci.* **109**, 509 (1996).
20. B. Mickey and J. Howard, *J. Cell Biol.* **130**, 909 (1995).
21. For 12 MTs, each over a 2-min interval, we measured the thermal fluctuations in the distance d between the middle of the MT and the line connecting the two ends of the MT: one end given by the position of the seed and the other end given by the position of the MT at length L, corresponding to the initial length of the MT (thus eliminating any sensitivity to changes in MT length during the measurement). An MT of length L can be viewed as two rigidly linked springs of length $L/2$, each with spring constant $24\kappa/L^3$. The total spring constant of this system is given by $48\kappa/L^3$. Given the equipartition theorem (*20*), the variance in d is connected to the flexural rigidity by
$$\kappa = k_B T L^3/[48\ \mathrm{var}(d)] \qquad (7)$$
Using this formula, we found $\kappa = 34 \pm 7$ pN·μm^2 (mean ± SD). Errors in this number could arise from measurement errors in the position of the ends and the middle of the MT. This is especially true when measuring short MTs, in which case noise may lead to an underestimation of the rigidity. The 12 MTs varied from 10 to 20 μm in length. No length dependence of κ was apparent over this range, but MTs shorter than 10 μm produced lower values for κ.
22. T. L. Hill, *Linear Aggregation Theory in Cell Biology* (Springer-Verlag, New York, 1987).
23. C. S. Peskin, G. M. Odell, G. F. Oster, *Biophys. J.* **65**, 316 (1993).
24. The elastic restoring force of a MT that is slightly buckled against an immobile barrier is roughly equal to f_c (*14*). This is still true when the end of the MT moves a small distance (relative to the length of the MT) away from the barrier because of thermal fluctuations. The force driving the gap between the MT end and the barrier to zero is therefore independent of the size of the gap. To leave a gap of size δ in the direction of MT growth, the MT end must be displaced by a distance $\delta \cos \phi$ against the buckling force f, where ϕ is the angle between the force and the growth direction of the MT. This is equivalent to saying that the MT end must be displaced by a distance δ against the component of the force f_p that is directed parallel to the axis of the MT. The contact angle with the wall does not play any role because the direction of the force is determined by the shape of the buckled MT, not by the normal to the wall. The Brownian ratchet model for a MT that grows by bending perpendicular to its axis is described in A. Mogilner and G. Oster, *Biophys. J.* **71**, 3030 (1996).
25. D. N. Drechsel, A. A. Hyman, M. H. Cobb, M. W. Kirschner, *Mol. Biol. Cell* **3**, 1141 (1992).
26. This does not exclude, of course, the possibility that force affects both rates. For instance, a fit to the function
$$v(f_p) = A \exp(-0.5Cf_p/\kappa) - B \exp(0.5Cf_p/\kappa) \qquad (8)$$
($q = 0.5$) produces a reasonable result as well: $\chi^2 = 0.43$ with $A = 1.20 \pm 0.05$ μm min^{-1}, $B = -0.007 \pm 0.010$ μm min^{-1}, and $C = 34 \pm 4$ μm^2. Note, however, that B is much smaller than A, implying that the effect of force is in any case dominated by a decrease in the on-rate, a result that is obtained for every positive value of q.
27. M. Dogterom, M.-A. Félix, C. C. Guet, S. Leibler, *J. Cell Biol.* **133**, 125 (1996).
28. A. A. Hyman, K. Middleton, M. Centola, T. J. Mitchison, J. Carbon, *Nature* **359**, 533 (1992).
29. T. E. Holy, M. Dogterom, B. Yurke, S. Leibler, *Proc. Natl. Acad. Sci. U.S.A.* **94**, 6228 (1997).
30. We thank T. E. Holy, S. Leibler, and K. Svoboda for discussions; K. Baldwin, T. E. Holy, and A. N. Pargellis for technical help; B. Shraiman and K. Svoboda for critical reading of the manuscript; and S. Leibler for use of his lab to prepare tubulin and MT seeds.

17 June 1997; accepted 17 September 1997

IKK-1 And IKK-2: Cytokine-Activated IκB Kinases Essential for NF-κB Activation

Frank Mercurio,* Hengyi Zhu, Brion W. Murray, Andrej Shevchenko, Brydon L. Bennett, Jian wu Li, David B. Young, Miguel Barbosa, Matthias Mann,

Anthony Manning, Anjana Rao

Activation of the transcription factor nuclear factor kappa B (NF-κB) is controlled by sequential phosphorylation, ubiquitination, and degradation of its inhibitory subunit IκB. A large multiprotein complex, the IκB kinase (IKK) signalsome, was purified from HeLa cells and found to contain a cytokine-inducible IκB kinase activity that phosphorylates IκB-α and IκB-β. Two components of the IKK signalsome, IKK-1 and IKK-2, were identified as closely related protein serine kinases containing leucine zipper and helix-loop-helix protein interaction motifs. Mutant versions of IKK-2 had pronounced effects on RelA nuclear translocation and NF-κB–dependent reporter activity, consistent with a critical role for the IKK kinases in the NF-κB signaling pathway.

Transcription factors of the NF-κB Rel family are critical regulators of genes that function in inflammation, cell proliferation, and apoptosis (*1*). The prototype member of the family, NF-κB, is composed of a dimer of p50 (NF-κB1) and p65 (RelA) (*2*). NF-κB exists in the cytoplasm of resting cells but enters the nucleus in response to various stimuli, including viral infection, ultraviolet irradiation, and proinflammatory cytokines such as tumor necrosis factor α (TNF-α) and interleukin-1 (IL-1) (*1, 3*).

Activation of NF-κB is controlled by an inhibitory subunit, IκB, which retains NF-κB in the cytoplasm (*4*). NF-κB activation requires sequential phosphorylation, ubiquitination, and degradation of IκB as well as consequent exposure of a nuclear localization signal on NF-κB (*5*). Ser^{32} and Ser^{36} of IκB-α, and the corresponding Ser^{19} and Ser^{23} of IκB-β, represent critical phosphorylated residues (*6*). The IκB kinase shows a high degree of specificity for these residues, because an IκB-α variant in which Ser^{32} and Ser^{36} were substituted by Thr (S32T, S36T) showed much reduced phosphorylation and degradation in stimulated cells and interfered with endogenous NF-κB activation (*6*).

To identify the IκB kinase responsible for the initial critical step of NF-κB activation, we fractionated whole-cell extracts (WCEs) from TNF-α–stimulated HeLa cells by standard chromatographic methods (*7*). We assayed IκB kinase activity in each fraction by phosphorylating glutathione-S-transferase (GST)–IκB-α (1–54) or GST–IκB-β (1–44) (*8*). Kinase specificity was established by using (S32T, S36T) mutant GST–IκB-α (1–54) [GST–IκB-α (1–54; S32T, S36T)], and GST–IκB-β (1–44), in which Ser^{19} and Ser^{23} were mutated to Ala [GST–IκB-β (1–44; S19A, S23A)] (*8*). IκB kinase activity was not observed in unstimulated cell extracts but was strong in cells stimulated for 5 to 7 min with TNF-α (*9*). Gel-filtration chromatography resolved this IκB kinase activity in a broad peak of 500 to 700 kD (Fig. 1A). In contrast to the 600-kD IκB kinase complex that was observed after treatment of cell extracts with either okadaic acid or ubiquitin-conjugating enzymes (*10*), the IκB kinase activity described here displayed no requirement for ubiquitination (*9*). We refer to the protein complex that contains the inducible IκB kinase activity as the IKK signalsome.

NF-κB activation occurs under conditions that also stimulate mitogen-activated protein kinase (MAP kinase) pathways (*11*). We tested preparations containing the IKK signalsome for the presence of proteins associated with MAP kinase and phosphatase cascades (Fig. 1B). The MAP kinase kinase–1 (MEKK-1) and two Tyr-phosphorylated proteins of ~55 and ~40 kD copurified with IκB kinase activity (Fig. 1B). A protein of ~50 kD that reacted with an antibody to MAP kinase phosphatase–1 (anti–MKP-1) also copurified with the IκB kinase through several purification steps.

F. Mercurio, H. Zhu, B. W. Murray, B. Bennett, J. Li, D. Young, M. Barbosa, A. Manning, Signal Pharmaceuticals, Inc., 5555 Oberlin Drive, San Diego, CA 92121, USA.
A. Shevchenko and M. Mann, European Molecular Biology Laboratory, Meyerhofstrasse 1, D-69012 Heidelberg, Germany.
A. Rao, Center for Blood Research and the Department of Pathology, Harvard Medical School, 200 Longwood Avenue, Boston, MA 02115, USA.

*To whom correspondence should be addressed. E-mail: fmercuri@signalpharm.com